

RSC Advances



This is an *Accepted Manuscript*, which has been through the Royal Society of Chemistry peer review process and has been accepted for publication.

Accepted Manuscripts are published online shortly after acceptance, before technical editing, formatting and proof reading. Using this free service, authors can make their results available to the community, in citable form, before we publish the edited article. This *Accepted Manuscript* will be replaced by the edited, formatted and paginated article as soon as this is available.

You can find more information about *Accepted Manuscripts* in the [Information for Authors](#).

Please note that technical editing may introduce minor changes to the text and/or graphics, which may alter content. The journal's standard [Terms & Conditions](#) and the [Ethical guidelines](#) still apply. In no event shall the Royal Society of Chemistry be held responsible for any errors or omissions in this *Accepted Manuscript* or any consequences arising from the use of any information it contains.



Mechanistic Insight of TiCl₄ Catalyzed formal [3+3] Cyclization of 1,3 –bis(silyl enol ethers) with 1,3-dielectrophiles

Received 00th January 20xx,
Accepted 00th January 20xx

DOI: 10.1039/x0xx00000x

www.rsc.org/

Riffat Un Nisa^a, Maria^a, Fatima Waseem^a, Tariq Mahmood^a, Ralf Ludwig^{b,c}, Khurshid Ayub^{*a}

The mechanism of TiCl₄ mediated formal [3+3] Cyclization of 1,3 –bis(silyl enol ethers) with 1,3-dielectrophiles is studied at B3LYP method of density functional theory (DFT) to rationalize the experimental regioselectivity. Methyl and trifluoromethyl substituted 1,3 dielectrophiles are studied theoretically since they show different regioselectivities. Two different mechanism involving 1,2 and 1,4 addition of 1,3 –bis(silyl enol ethers) on 1,3-dielectrophiles are studied for each dienophile. The intramolecular transition metal catalyzed and non-catalyzed dynamic shift of silyl moiety is also studied. The structure of 1,3 dienophile and the associated Mullikan charges are the driving forces for different regioselectivities in methyl and trifluoromethyl dienophiles.

Introduction:

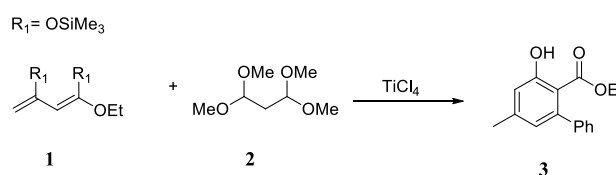
Functionalized arenes are interesting class of organic molecules in natural products[1], polymers [2] and medicinal chemistry [3]. The traditional approaches for substituted arenes synthesis involve direct substitution of already existing benzene scaffold. The widely used strategies based on this classical approach involves electrophilic [4], nucleophilic substitution [5] (in case of aryl halide) and transition metal catalyzed coupling reactions[6]. However, these strategies suffers from some serious drawbacks such as activating/deactivating effects of electron-donating /withdrawing groups[7], sequences of multistep reaction, low yields and decreased availability of functionalized arenes as starting materials [7, 8]

A significant alternative method is the “acyclic approach” for the synthesis of highly functionalized arenes, which are based on acyclic precursors [8]. These cyclocondensation reactions include [3 + 2 + 1] Dötz reaction [9], transition metal catalyzed [2 + 2 + 2] cyclisation, [4 + 2] cycloadditions [10], [4 + 2] Danheiser alkyne-cyclobutenone cyclization [11], 1,6-electrocyclization reactions [12], cyclocondensations of dielectrophiles with dinucleophiles and

[5 + 1] benzannulations between alkenoyl keteneacetals and nitroalkanes [13]. However, these annulations proceeds in harsh reaction conditions, require highly expensive catalysts, suffers from regiochemical ambiguities and lack of substrate generality [8].

The [3 + 3] addition of 1,3-bis(silyloxy)-1,3-butadienes with 3-silyloxy-2-en-1-ones is an important TiCl₄ mediated one pot cyclization reaction based on the “acyclic approach” [14]. The significance of the reaction includes its high regioselectivity [14], excellent yields, moderate reaction conditions, and commercial availability of the catalyst[15, 16]. TiCl₄ is an efficient Lewis acid and shows significant affinity for oxygen containing organic compounds. The catalyst is effective in many organic transformations [17], particularly in Pinacol coupling reaction [18], pyrrolidine synthesis [19], Claisen rearrangements [20], and asymmetric aldol reaction [21]. The alkene production from molecular reductive coupling of carbonyl compounds such as aldehydes, ketones, acylsilanes, ketoesters, and oxoamides are also prominent applications of titanium in organic chemistry [17].

Chan and coworkers (in 1979) reported the synthesis of arenes by formal [3+3] cyclization of 1,3 –bis(silyl enol ethers) with 1,3-dielectrophiles, using titanium (IV) as a lewis acid (Scheme 1)[22]. The reaction is widely used for synthesis of valuable functionalized arenes[7]. For example, Lewis acid promoted reaction of 1,3-bis(silyl enol ether) **1** with **2** delivers functionalized biphenyl compound **3**.



Scheme 1. TiCl₄ catalyzed cyclization of 1,3 bis(silyl enol ether) with 1,1,3,3-tetramethoxypropane.

^a Department of Chemistry, COMSATS Institute for Information Technology, Campus Abbottabad, Abbottabad, Pakistan

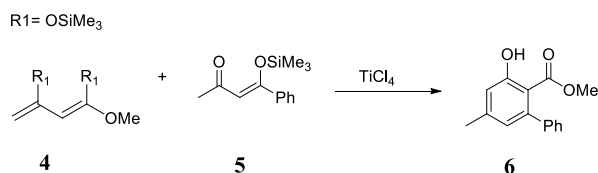
^b Leibniz-Institut für Katalyse e. V. an der Universität Rostock, Albert-Einstein-Str. 29a, 18059 Rostock, Germany

^c Department of Physical Chemistry, University of Rostock, Dr.-Lorenz-Weg 1, 18059 Rostock, Germany

^a Fax = +92-992-383441 khurshid@ciit.net.pk

† Footnotes relating to the title and/or authors should appear here.

Electronic Supplementary Information (ESI) available: Total electronic, zero-point and Gibbs free energies alongwith the cartesian coordinates of the optimized geometries are shown in the supplementary information. Supplementary data associated with this article can be found, in the online version, See DOI: 10.1039/x0xx00000x

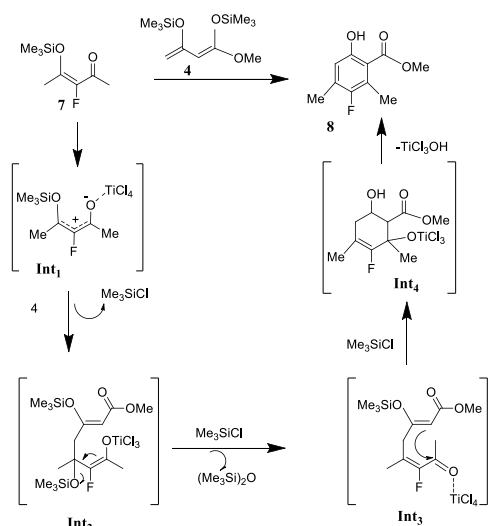


Scheme 2. TiCl₄ catalysed regioselective [3 + 3] addition of 1,3-bis(silyloxy)-1,3-butadienes with 3-silyloxy-2-en-1-ones

Similarly, A similar biphenyl derivative **6** can be generated (Scheme 2) by the reaction of 1,3-bis(silyl enol ether) **4** and 3-silyloxy-2-en-1-one **5**.

Despite much synthetic advancement, mechanistic details of formal [3+3] cyclization are very limited. A proposed mechanism by Langer and coworkers[7] is presented in scheme 3. TiCl₄ selectively activates one of the two electrophilic centers of the unsymmetrical 1,3-dielectrophile by forming six membered chelation ring, which leads to the formation of exclusively one isomer and results in regioselective cyclization. Nature of the Lewis acid also affects the reaction pathway because specific functional groups are activated by specific Lewis acid.

The proposed mechanism involves coordination of **7** with TiCl₄ to give intermediate **Int1**, which is then attacked by the terminal carbon atom of **4** to give intermediate **Int2**. The **Int2** loses OSiMe₃ moiety to deliver **Int3**. Cyclization of **Int3** followed by aromatization in **Int4** deliver a functionalized arene **8** (Scheme 3). The above mechanism allows to rationalize the regioselectivity of a particular formal [3+3] reaction, however, it is relatively silent regarding the different regioselectivities starting from two structurally similar substrates (Scheme 4, vide infra). Moreover, the mechanism is based on a 1,4 addition of 1,3-bis(silyloxy)-1,3-butadienes on 1,3-dienophile. A competitive 1,2 addition is not invoked in the mechanism.



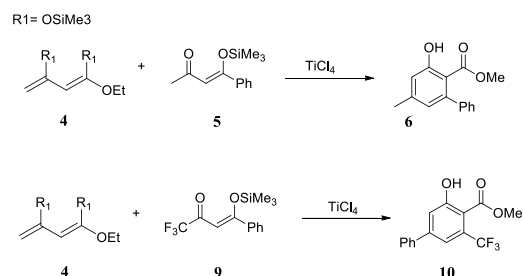
Scheme 3. Proposed mechanism of TiCl₄ catalysed 3 + 3 addition of 1,3-bis(silyloxy)-1,3-butadienes with 3-silyloxy-2-en-1-ones

With the computational tools in hand, we became interested to investigate the mechanism of the formal [3+3] addition and the results are presented here. There appears no theoretical reports on the mechanism of the titanium catalyzed [3 + 3] addition of 1,3-bis(silyloxy)-1,3-butadienes with 3-silyloxy-2-en-1-ones.

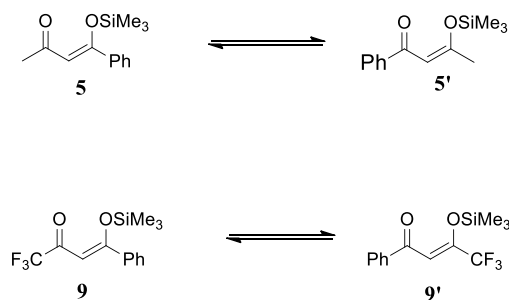
Computational Methods

All calculations were performed with Gaussian 09. Geometries of the structures were optimized without any symmetry constraints at hybrid B3LYP method using 6-31G* basis set. The B3LYP method consists of three parameter hybrid functional of Becke in conjunction with the correlation functional of Lee, Yang, and Parr. The B3LYP method provides a nice balance between cost and accuracy, and it is known to perform reasonably well for the prediction of geometries and behaviour of neutral and charged species[23] including transition metals. The B3LYP method has been used in the theoretical simulations of properties and reactions catalysed by Titanium[24]. Each optimized structure was confirmed by frequency analysis at the same level (B3LYP/6-31G*) as a true minimum (no imaginary frequency) or a transition state (with one imaginary frequency). Imaginary frequencies of transition states were also evaluated to confirm that their associated eigenvector correspond to the motion along the reaction coordinates. Moreover intrinsic reaction coordinates (IRC) calculations were performed to confirm that the transition states connect to the concerned starting materials and products. IRC was performed until the stationary point was reached with RMS gradient less than 1×10^{-4} . Stationary points located through IRC were then fully optimized at the above mentioned method. The reported energies for all structures are in kcal mol⁻¹ and include unscaled zero point energy corrections.

Density functional theory (DFT) calculations were performed to gain mechanistic insight for the regioselectivity observed for the [3 + 3] addition of 1,3-bis(silyloxy)-1,3-butadienes with 3-silyloxy-2-en-1-ones (Scheme 4). An *ortho* phenyl substituted benzoate ester **6** is the dominant product from **5** (a methyl ketone) whereas *para* phenyl substituted benzoate ester **10** is the major product from **9**. The regioselectivity is altered when methyl ketone is replaced with a trifluoromethyl ketone, **9**. A number of questions needs to be answered in order to logically investigate the mechanism; Is the silyloxy group in dielectrophiles **5** and **9** dynamic between the two oxygen atoms (**5** → **5'** and **9** → **9'**)? If yes, then which isomer is more stable? What is the stability order for these two isomers when they are bound to titanium? Is it a direct addition of **4** on **5**, or a 1,4 addition?



Scheme 4. Illustration of observed regioselectivities in [3 + 3] addition of 1,3-bis(silyloxy)-1,3-butadienes with 3-silyloxy-2-en-1-ones



Scheme 5. Reversible silyl shifts between oxygens of 3-silyloxy-2-en-1-ones

Therefore, in this study, we have attempted to address all these questions and the results are described below. However, to reduce the computational cost, SiMe₃ group is replaced with SiH₃.

Shift of the silyl group

α , β unsaturated ketones **5** and **9** can exist in isomeric species **5'** and **9'**, respectively by the shift of the silyl group between two oxygen atoms (Scheme 5). The dynamic shift is studied both in the presence and absence of the transition metal (Ti) and it is observed that the shift of the silyl group both in fluorinated and non-fluorinated substrates, **9** and **5**, respectively, is a kinetically favourable process even in the absence of the transition metal (titanium). A transition state for the silyl shift in **2** is located at a barrier of 2.91 kcal mol⁻¹ from **5** (titanium free conditions), and the reaction is exothermic by 0.36 kcal mol⁻¹. The low activation barrier for the silyl shift may be attributed to the close proximity of the silyl group to the keto oxygen in **5**. The O1-Si bond (see Figure 1 for numbering) in the transition state slightly increases to 1.89 Å compared to 1.73 Å in **5** (Figure 2). The O1-Si bond in the product **5'** is 2.27 Å. On the other hand, the O2-Si bond decreases to 1.88 Å in **TS1** from 2.22 Å in **5**, and finally to 1.74 Å in **5'**. The stronger bond of silicon with both oxygen atoms may be another reason for low activation barrier

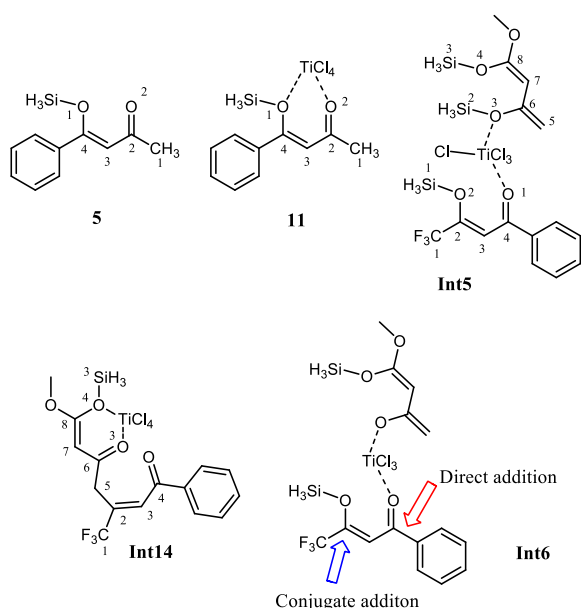


Figure 1. Numbering scheme for discussion, and description of 1,2 and 1,4 addition

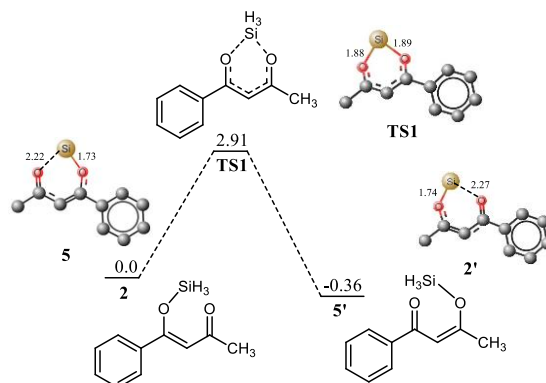


Figure 2. Potential energy diagram for silyl shift between **5** and **5'**. All values are relative to **5** at 0.0 kcal mol⁻¹. All bond distances are in Angstroms. Unnecessary hydrogen atoms are removed for clarity

A similar behaviour is also observed for the fluorinated substrate **9**. A transition state (Figure 3) for silyl shift is observed at a barrier of 4.06 kcal mol⁻¹, and the reaction is exothermic by 0.9 kcal mol⁻¹. A relatively higher activation barrier from **9** (compare **5**→**5'**) may be attributed to the electron withdrawing effect of the CF₃ functional group which decreases the electron density on the keto oxygen. Therefore, the nucleophilic attack of the keto oxygen on the silyl group is relatively difficult. The shift of the silyl group in **4** and **9** is kinetically a favourable process even in the absence of transition metal.

Complexation with Titanium

Phenyl ketones **5'** and **9'** are more stable compared to their alkyl/trifluoroalkyl ketones **5** and **9**, respectively, therefore, compounds **5'** and **9'** are anticipated as active species in the reaction. However, the situation is somewhat different after complexation with titanium. Although **5'** is more stable than **5**; however, its titanium tetrachloride complex **11'** is relatively unstable by 2 kcal mol⁻¹ compared to **11**, a complex from **5**. The greater stability of **11** relative to **11'** can be explained on the basis of attractive interaction between the hydrogens of CH₃ with the chlorides of TiCl₄. H—Cl bond distances are 2.89 Å and 2.85 Å (Figure 4).

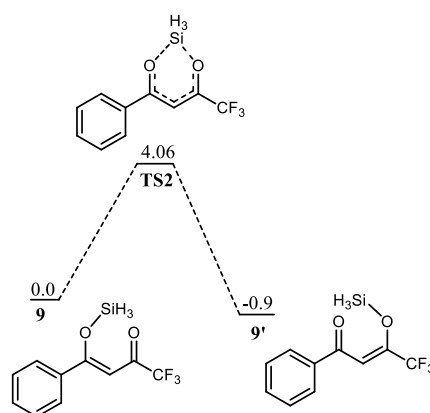


Figure 3. Potential energy diagram for silyl shift between **9** and **9'**. All values are relative to **9** at 0.0 kcal mol⁻¹.

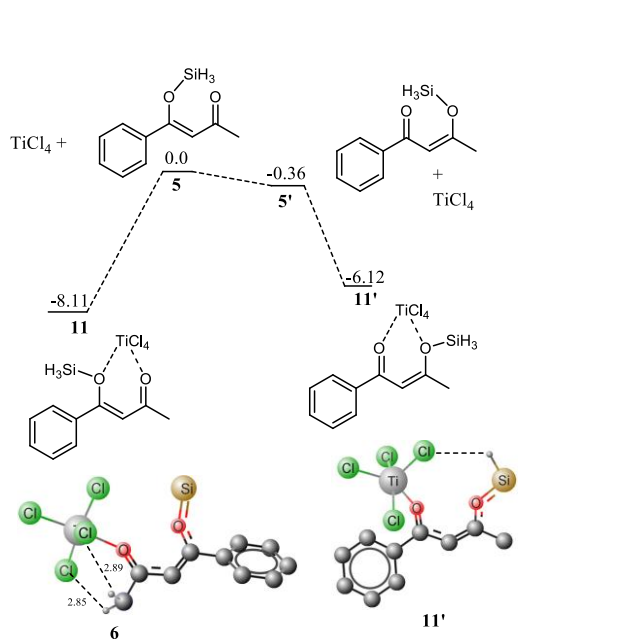


Figure 4. Potential energy diagram for complexation of **5** and **5'** with titanium to deliver **11** and **11'**, respectively. All values are in kcal mol⁻¹ with respect to **5** at 0 kcal mol⁻¹. All bond lengths are in Angstroms, and unnecessary hydrogen atoms are removed for clarity

For **9**, this reversal of stability on complexation with titanium is not observed. The complex of **9'** with titanium (**12'**) is still more stable than **12** by 0.38 kcal mol⁻¹. The higher stability of **12'** over **12** is supportive to our hypothesis above that interaction of hydrogen of CH₃ with the chlorides of TiCl₄ is the main driving force for the higher stability of **11** over **11'**. The attractive interactions (CH₃---Cl) in **11** are replaced by repulsive interactions in **12** (CF₃ with chlorides). These interactions are shown in Figure 5.

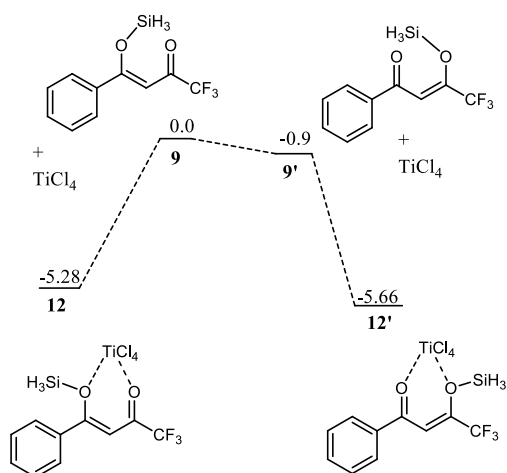


Figure 5. Potential energy diagram for complexation of **9** and **9'** with titanium to deliver **12** and **12'**, respectively. All values are in kcal mol⁻¹ with respect to **9** at 0 kcal mol⁻¹.

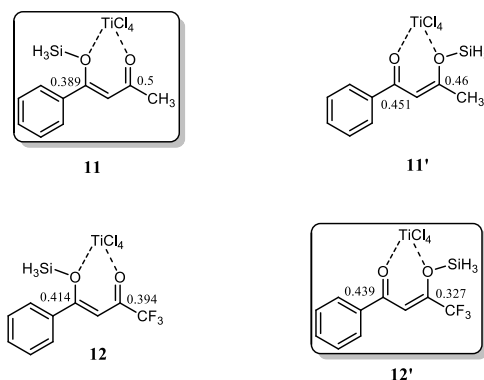


Figure 6. Mulliken charges analyses on carbon 2 and 4 in **11**, **11'**, **12** and **12'**.

In the next step of our mechanistic investigation we analyzed the distribution of charges in **11**, **11'**, **12** and **12'** (shown in figure 6) in order to predict the reactivity based on charge densities. In both **11** and **11'**, the position of highest positive charge density is the carbon bearing the methyl group regardless of the fact whether this carbon is a keto carbon or silyloxy bearing carbon. In **11**, C2 and C4 (see figure 1 for labelling) have 0.5 and 0.389 positive charges, respectively whereas in **11'**, C2 and C4 bear 0.46 and 0.45 positive charges respectively. Since **11** is more stable and has higher positive charge on methyl ketone carbon therefore we believe that this isomer will be the active participating species in the reaction. For the fluorinated arene **12**, the situation is quite opposite; a high positive charge is observed on carbon bearing the phenyl ring (C4). In **12'**, carbons 2 and 4 have 0.327 and 0.439 positive charges, respectively whereas in **12**, carbons 2 and 4 bear 0.394 and 0.414 positive charges, respectively. It is interesting to note that both isomers (of any system) have similar sequence of charge distribution.

Discussion in the subsequent section has been divided into fluorinated and methyl systems, and in each section 1,4 and 1,2 addition are discussed in detail

Fluorinated 1,3 dielectrophile

1,2 Addition

The bis silyl ether **4** contains two oxygen atoms which are available for binding with titanium therefore, it is believed that the bis silyl ether binds to **12** before the reaction takes place. The titanium is penta coordinated in **12'** and the binding of **4** with titanium of **12** would generate an octahedral complex, **Int5**. Coordination of oxygen with titanium is followed by loss of the silyl chloride (Scheme 4). The literature reveals that octahedral complexes of titanium are well known and are quite stable [25, 26].

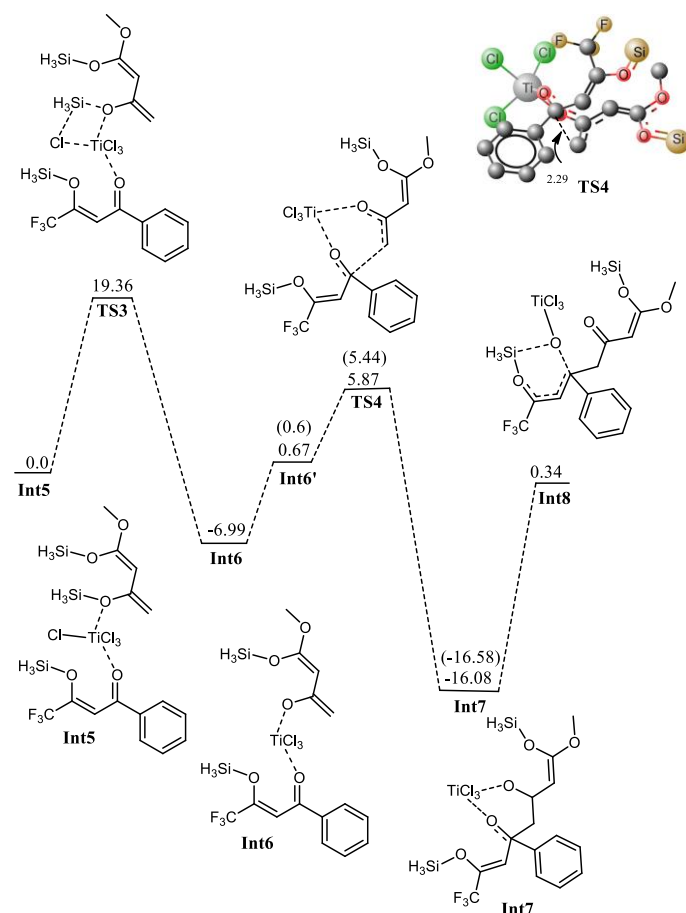


Figure 7. Potential energy diagram for elimination of $\text{H}_3\text{Si-Cl}$ followed by C-C bond formation (**Int5** \rightarrow **Int8**); All energies are relative to **Int5** at 0 kcal mol⁻¹. All bond lengths are in Angstroms. Unnecessary hydrogen atoms are removed for clarity. Values in parenthesis correspond to trimethylsilyl substituted derivatives.

Complexation of **4** with **12'** generates an intermediate octahedral complex **Int5** where both oxygen atoms are in *cis* orientation. O1-Ti and O3-Ti bond lengths are 2.12 and 2.38 Å, respectively. The large bond distance of siloxy-Ti may be due to steric reasons (Figure 7). The chlorides-Ti bonds *trans* to oxy ligands are relatively short (2.24 Å) whereas other Ti-Cl bonds are somewhat elongated (2.28 and 2.32 Å, shown in Figure 8). The *cis* orientation of the oxy ligands is necessary for subsequent addition reaction. Any *trans* orientation of these group will not be favourable for C-C bond formation. A chloride ligand on titanium in **Int5** is parallel to the silyl group at a distance of 3.29 Å.

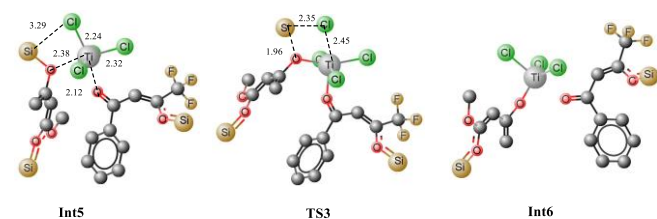


Figure 8. Optimized geometries of **Int5**, **TS3** and **Int6**. All bond lengths are in Angstroms, and unnecessary hydrogen atoms are removed for clarity

A transition state for the concomitant elimination of the silyl and chloride groups is located at a barrier of 19.36 kcal mol⁻¹. The transition state (**TS3**) has the geometry very similar to **Int5** except the bond lengths change at the reaction site. The Ti-Cl bond elongates to 2.45 Å in **TS3** from 2.24 Å in **Int5**. Cl-Si and O3-Si2 bond distances are 2.35 and 1.96 Å, respectively in the transition state. The reaction has low activation barrier, and easily accessible at room temperature. Moreover this step is also driven thermodynamically. The product of the reaction, **Int6** is 6.96 kcal mol⁻¹ more stable than the starting material (**Int5**). The loss the silyl group generates an oxy ligands which is very well suited for the nucleophilic attack on the α,β unsaturated ketone moiety to generate C-C bond. In the product **Int6**, both organic ligands are not well suited for C-C bond formation. Conformational changes are required to bring both organic fragments in proper orientation for C-C bond formation. This conformational change costs 7.66 kcal mol⁻¹. A transition state is located at a barrier of 5.2 kcal mol⁻¹ from **Int6'**. This low activation energy may be attributed to relative higher positive and negative charge densities on C4 and C6 carbons, respectively. The C-C bond being formed has a bond length of 2.29 Å in the transition state. Some other bond lengths also change considerably during the C-C coupling reaction. The O3-Ti bond length increases from 1.78 Å in **Int6'** to 1.90 Å in the **TS4** whereas the O1-Ti bond length decreases from 2.06 to 1.94 Å.

Since we have replaced the trimethylsilyl group with SiH3 in order to reduce the computational cost, it was of interest whether this simplification affects the activation barriers, and may change the regioselectivities. Towards this end, activation barriers for the key step (1,2 or 1,4 (vide infra)) are studied with $\text{Si}(\text{CH}_3)_3$ groups as well and the activation barriers are given in the parenthesis (see Figure 7 and Figure 10). It is very obvious from Figure 7 that the activation barrier is not affected considerably by replacing trimethylsilyl (4.84 kcal mol⁻¹) group with SiH3 (5.20 kcal mol⁻¹).

Int7 is believed to undergo an interesting rearrangement of OTiCl₃ to the silyl group which subsequently delivers **Int9** by elimination of TiCl₃(OSiH₃). Although transition state for this oxy-titanium shift is located for methyl system (vide infra); however, no such transition state is located for fluorinated analogue. Rather, a true minimum **Int8** is observed in which oxytitanium is bound to both, silyl moiety and carbon 5. The O3-C5 and O3-Si1 bond distances are 2.66 Å and 3.04 Å, respectively. Thermodynamic cost for this shift is 16.42 kcal mol⁻¹. **Int9** undergoes coordination of the 2nd silyloxy oxygen (O4), which is followed by elimination of another Si and Cl, very similar to the one observed in **Int5**. The transition state for the elimination of silyl chloride (**TS5**) is not modelled here. The activation barrier for the elimination of silyl chloride, is believed similar to the one observed in **Int5**. The product of the silyl chloride elimination, **Int10** undergoes nucleophilic attack on the CF₃-CO group. Kinetic barrier for the step is 26.56 kcal mol⁻¹. The reaction is also favourable thermodynamically; the product (**Int11**) lies 18.7 kcal mol⁻¹ lower in energy than **Int10** (Figure 9). The cyclized product is believed to undergo loss of a water molecule and finally tautomerization to deliver the product. The possibility of elimination of silyl chloride with concomitant cyclization to deliver the final product cannot be excluded safely.

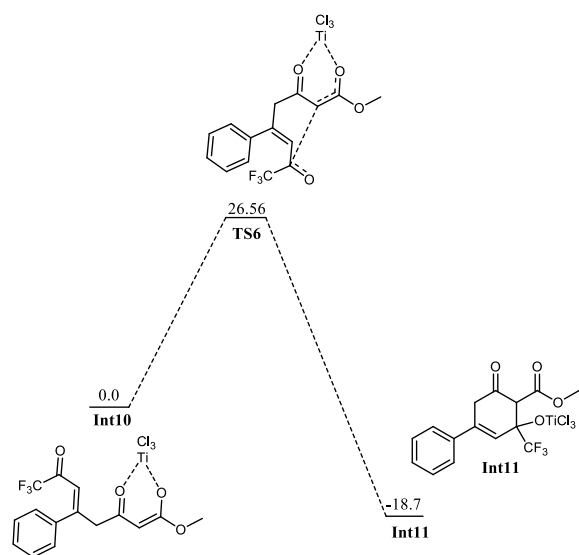


Figure 9. Potential energy diagram for cyclization in **Int10** to generate **Int11**. All energies are in kcal mol^{-1} relative to **Int10** at $0.0 \text{ kcal mol}^{-1}$.

1,4 addition

The competitive reaction for **Int6'** is 1,4 addition on enone fragment instead of a 1,2 addition. The activation barrier for C-C bond formation through 1,4 addition was found higher compared to the 1,2 attack; $13.10 \text{ kcal mol}^{-1}$ for 1,4 addition compared with $5.2 \text{ kcal mol}^{-1}$ for the 1,2 attack. The higher activation barrier for **Int6' → Int12** (Figure 10) compared to **Int6-Int6' → Int7** may be due to steric crowding at the carbon bearing the siloxy and CF_3 moieties, or may be due to electronic factors because of reduced charge density at keto carbon C2. The C6-C2 bond distance is 2.39 \AA in the transition state (**TS7**), compared to 2.29 \AA in the transition state for the 1,2 attack, **TS4**. The titanium has trigonal bipyramidal geometry in **TS7** where fluorine atoms of CF_3 do not coordinate to the titanium. The reaction is thermodynamically favourable ($E_R = 16.12 \text{ kcal mol}^{-1}$). The activation barrier for the similar reaction but involving $\text{Si}(\text{CH}_3)_3$ has a very similar activation barrier ($12.37 \text{ kcal mol}^{-1}$). These findings are consistent with those in Figure 7 that replacing a trimethylsilyl group with SiH_3 does not change the activation barrier to alter the regioselectivities.

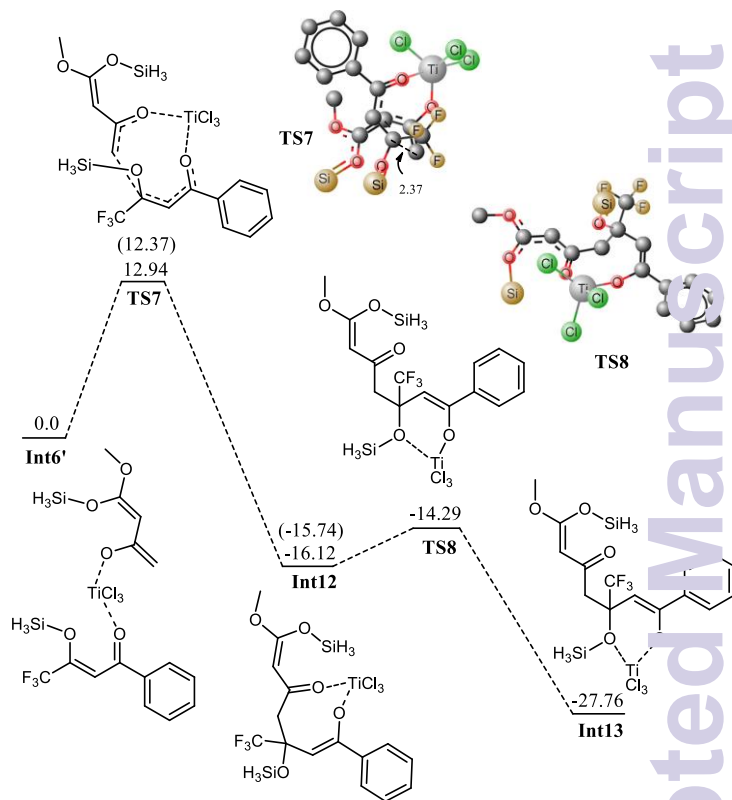


Figure 10. Potential energy diagram for 1,4 addition in **Int6'** to generate **Int12**, followed by change in coordination to generate **Int13**. Hydrogen atoms are removed for clarity. All bond lengths are in Angstroms. Values in parenthesis correspond to trimethylsilyl substituted derivatives

Int12 undergoes elimination of O-SiH_3 (next to CF_3) and TiCl_3 moiety to generate the species for the next step, **Int13**. This process may be a direct one step process for the methyl ketone (vide infra) or may be a multistep process as in the case of trifluoro species. For the trifluoro species, first the silyl oxygen coordinates to titanium and a transition state **TS8** has been located for this coordination. This is just an addition reaction because it does not involve elimination of any other group. The cyclic species undergoes cleavage of OSiH_3 and TiCl_3 to generate **Int14** (see supporting information). In **Int14**, a silyl group is parallel to a chloride on titanium therefore; elimination of silyl chloride generates the enoxy species **Int15**. The geometry of **Int15** has some interesting features; C7 is coordinating with titanium at a distance of 2.34 \AA , the carboxylate oxygen (O4) along with the *ortho* carbon C7 behave as bidentate ligand for titanium, the titanium in **Int15** has distorted octahedral geometry. Nucleophilic attack of C7 on C4 in **Int15** generates the cyclic species **Int16**. The reaction has kinetic demand of $33.20 \text{ kcal mol}^{-1}$ (Figure 11). In the transition state, C7-C4 bond distance is 2.68 \AA whereas the C-Ti distance is increased to 2.75 \AA . Although kinetically unfavourable, the reaction is highly favourable thermodynamically. The reaction is exothermic by $19.32 \text{ kcal mol}^{-1}$. Thermal energy available at room temperature is not sufficient to surpass this barrier which clearly illustrates that this is not the pathway which should be observed experimentally. The regioselectivity observed experimentally is in marked contradiction with the product obtained from 1,4 addition.

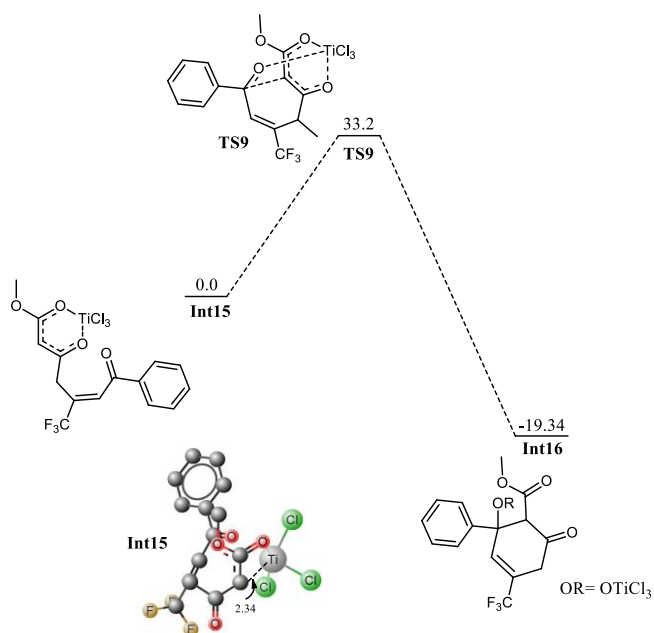


Figure 11. Potential energy diagram for intramolecular cyclization in **Int15** to generate **Int16**, all energy values are relative to **Int15** at 0.0 kcal mol⁻¹. Hydrogen atoms are removed for clarity All bond lengths are in Angstroms

The 1,2 addition is a favourable pathway energetically, and it explains the right regioselectivity. Although the calculations above reveal that 1,2 attack of enol on the keto oxygen delivers the product which is observed experimentally yet there is another set of similar calculations but with CF₃ ketone bound to titanium in the first step rather than a phenyl ketone. We have also considered this as a possible reaction in our study.

1,2 attack on CF₃ Ketone

Calculations have been performed on a titanium bound complex starting from CF₃ ketone, **Int17**. Typically the nature and the number of step are almost comparable to those for phenyl ketone regarding both 1,2 and 1,4 attack. We have repeated the same set of calculations for CF₃ ketone to explore the associated kinetics and thermodynamics. The first step is elimination of silyl chloride from **Int17** for which a transition state has been located at a barrier of 19.67 kcal mol⁻¹ from starting complex. The activation barrier is very comparable to the elimination of silyl chloride in **Int5** (19.36 kcal mol⁻¹). The reaction is thermodynamically favourable by 8.52 kcal mol⁻¹. A few important changes in bond distances on going to transition states are given in the table below.

Table 1. Comparison of some important geometric parameters in **Int17** and **TS10**

Bond	Int17	TS10
Ti-Cl	2.24	2.45
Ti-O	2.36	2.00
O-Si	1.72	1.95
Si-Cl	3.31	2.35

Nucleophilic attack of enol on the C2 in **Int18'** is a kinetically favourable (E_{act} 6.22 kcal mol⁻¹, see Figure 12) but this activation energy is slightly higher (1 kcal mol⁻¹) compared to the activation barrier for nucleophilic attack on phenyl ketone **Int6** (E_{act} = 5.2 kcal mol⁻¹). This difference in activation barrier may be attributed to the density of the positive charge of **12'** and **12** (vide supra). The important C6-C2 bond (being formed) has bond length of 2.37 Å in the transition state **TS11** compared to 3.61 Å and 1.54 Å in **Int19** and **Int18**, respectively. The similar reaction using Si(CH₃)₃ group instead of SiH₃ has the activation barrier of 6.63 kcal mol⁻¹ (see supporting info, Figure S11)

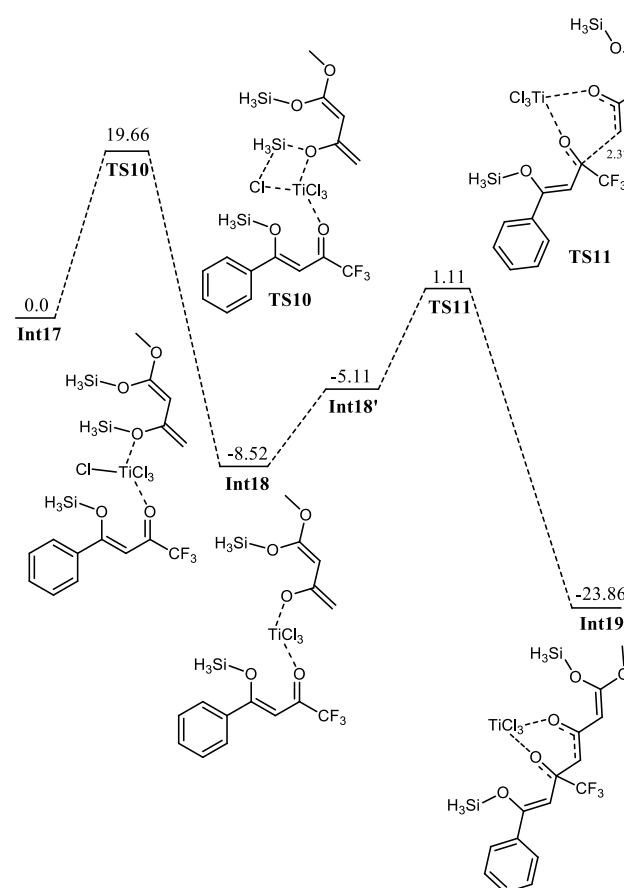


Figure 12. Potential energy diagram of Ti catalyzed 1,2 addition of enol on CF₃ ketone, All values are in kcal mol⁻¹ relative to **Int17** at 0.0 kcal mol⁻¹.

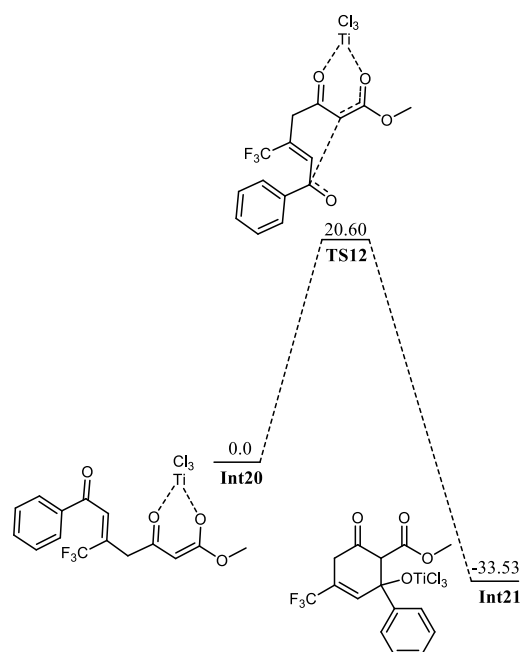


Figure 13. Potential energy diagram for cyclization in **Int20**. All values are in kcal mol⁻¹ relative to **Int20** at 0.0 kcal mol⁻¹

The next key step in this pathway is the cyclization of **Int20** to **Int21**, a reaction which generates the cyclic intermediate (**Int21**) from enol by nucleophilic attack (Figure 13). The calculated activation barrier for the cyclization is 20.60 kcal mol⁻¹. This activation barrier is although high but still accessible under the reaction conditions. Although energetics associated with this pathway are not very high (may proceed under reaction conditions); however, its comparison with 1,2 attack on phenyl ketone (1,2 attack starting from **Int6**) shows that this pathway is energetically less favourable. Moreover, the theoretical findings are consistent with the experimental regioselectivities (compare the structure of **Int21** and **Int11** with **Int10**).

The 1,4 attack on CF₃ ketone is expected to be kinetically demanding, although it delivers the desired product. The 1,4 addition on CF₃ ketone is also modelled, and found to have high activation barriers (See Figures S12 and S13). The first 1,4 attack has an activation barrier of 15.99 kcal mol⁻¹ (much higher than any of the above three mechanisms). This high activation barrier is expected because this reaction not only involves 1,4 attack which is kinetically demanding but it involves intermediate **18'** on which attack is even more demanding kinetically. Analysis of the pathways, shown above, clearly indicates that the charge density shown in Figure 6 is a good tool to predict the regioselectivity of the reaction. Moreover, pathways with 1,2 attack on ketone are energetically more favourable whereas conjugate addition is thermodynamically less favourable.

Methyl system

From Figure 6, it is apparent that the methyl ketone **11** has higher Mulliken charge density on C2; therefore, this structure is only considered for mechanistic studies. The phenyl ketone **11'** is not considered for both 1,2 and 1,4 attack because higher activation barriers are expected than **11** (vide supra). Moreover, the

regioselectivity expected through a 1,2 attack is in contradiction to what is observed experimentally.

1,2 attack

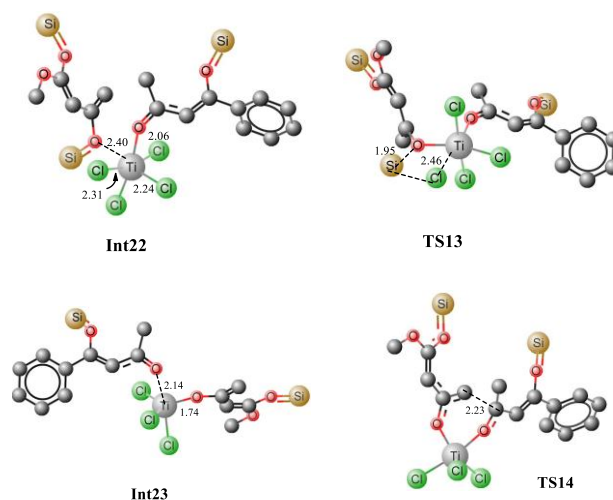


Figure 14. Optimized geometries of **Int22**, **TS13**, **Int23** and **TS14**. Unnecessary hydrogen atoms are removed for clarity. All bond lengths are in Angstroms

The first step is typically cleavage of a chloride and a silyl group in **Int22**. The titanium in **Int22** has an octahedral geometry where both oxygen ligands are *cis* to each other. The O3-Ti-O2 bond angle is 81.77 degrees. The O3-Ti and O2-Ti bond distances are 2.40 and 2.06 Å, respectively. The Ti-Cl (*trans* to oxy ligands) bond lengths are in the range of 2.24-2.25 Å whereas the other chloride-titanium bond lengths are 2.30-2.31 Å. One of the chlorides is bent towards silyl group primarily because of the dipole-dipole interactions (Figure 14). A transition state for the cleavage of silyl chloride in **Int22** is located at a barrier of 18.74 kcal mol⁻¹ from **Int22**, See Figure 15). In the transition state **TS13**, Cl-Ti bond distance increases to 2.46 Å. The alkoxide-titanium bond distance decreases to 2.01 Å in **TS13**. The geometry on titanium also changes. The Cl-Ti-O3 (silyl) angle drops to 159.0 degrees in **TS13** from 176.18° in **Int22**. This activation barrier for the cleavage of a silyl and a chloride is very comparable to the one observed for the trifluoro system (vide supra). These findings clearly illustrate that the cleavage is not significantly influenced by the structure of the complex. The reaction is exothermic by 6.5 kcal mol⁻¹. The complex **Int23** has trigonal bipyramidal geometry around titanium. The two chlorides and alkoxide ligands do not make a perfect trigonal planar structure. O-Ti-Cl bond angles are 114-115 degrees, whereas Cl-Ti-Cl bond angle is 127.65 degrees. Two chlorides and the alkoxide ligands are in one plane (trigonal). The third chloride and ketone oxygen are in the perpendicular plane. The alkoxide-Ti and ketone-titanium bond distances are 1.74 and 2.14 Å, respectively. The subsequent C-C bond formation in **Int23** has kinetic demand of 11.23 kcal mol⁻¹, whereas the reaction is thermodynamically favourable by 12.03 kcal mol⁻¹. In the transition state, the C2-C6 bond distance is 2.23 Å. Moreover, the O3-Ti and O3-C5 bond distances are 1.88 and 1.31 Å, respectively. The newly formed O2-Ti and C2-O2 bond distances are 1.94 and 1.30 Å, respectively. The **Int23**, generated as a result of C-C bond formation, undergoes an interesting cleavage/shift of titanium oxy group on the silyl group. This shift is predicted to have a kinetic demand of 19.12 kcal mol⁻¹

In the transition state, O1-C2 bond distance is 2.15 Å whereas the O2-Si1 bond distance is 3.17 Å.

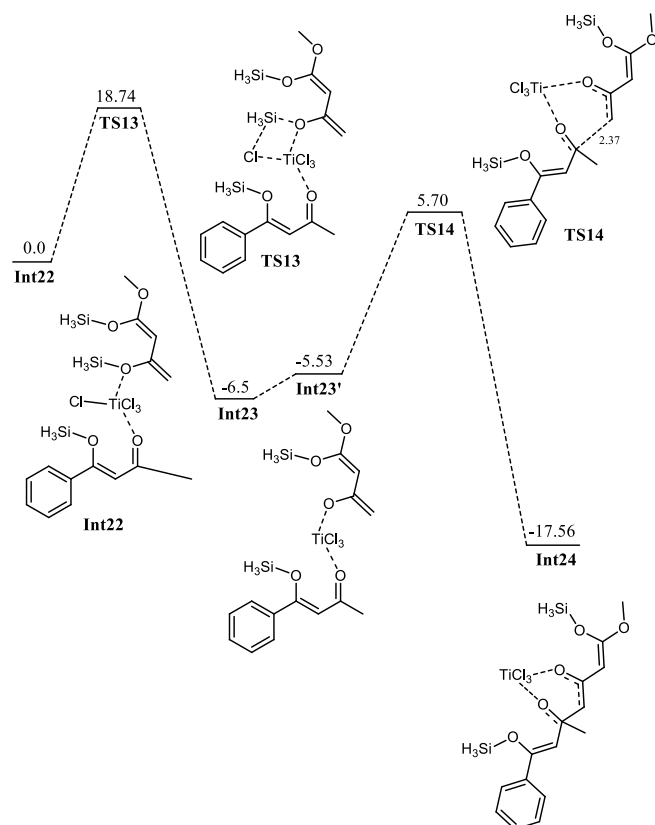


Figure 15. Potential energy diagram for elimination of silyl chloride followed by 1,2 addition of enol to methyl ketone to generate **Int24**. All values are in kcal mol⁻¹ relative to **Int22** at 0.0 kcal mol⁻¹

The titanium oxy group interacts very loosely with the silyl groups, as it is reflected with bond separation in the TS. This behaviour of the methyl system is remarkably different than what is observed for the trifluoromethyl analogue. In the case of trifluoromethyl system, this type of transition state is not observed rather an intermediate is observed in which titanium oxy species is located between carbon and silyl group (vide supra)

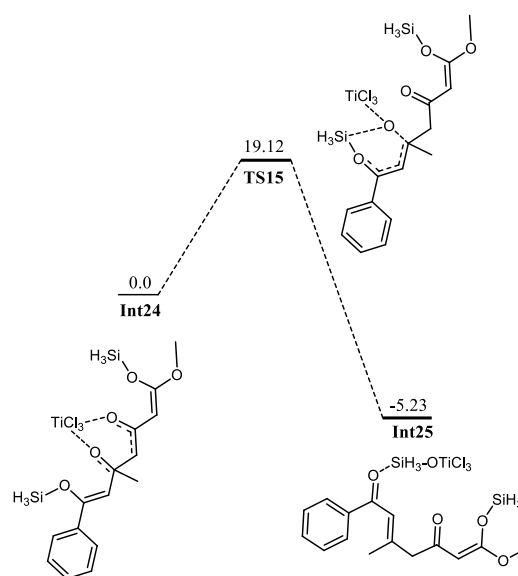


Figure 16. Potential energy diagram for migration of OTiCl₃ to silyl moiety in **Int24** to generate **Int25**. All values are in kcal mol⁻¹ relative to **Int24** at 0.0 kcal mol⁻¹

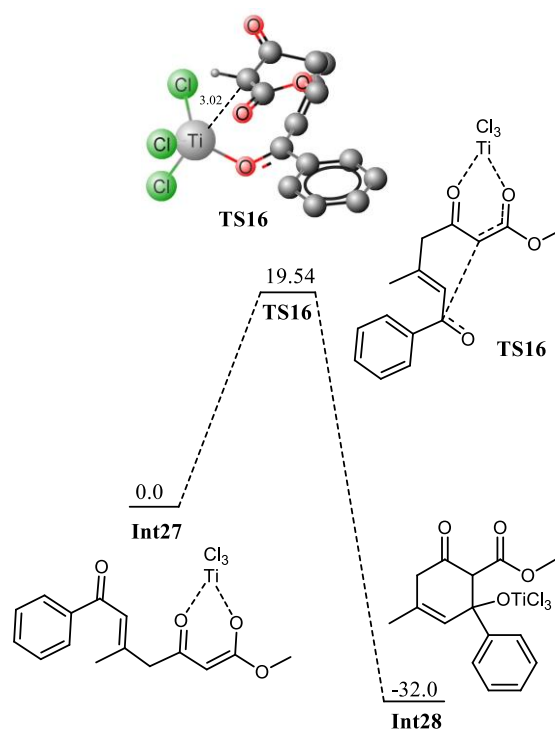


Figure 17. Potential energy diagram for cyclization in **Int27**. All values are in kcal mol⁻¹ with respect to **Int27** at 0.0 kcal mol⁻¹

It is believed that the **Int25** generated in the above step (Figure 16) soon loses Cl₃Ti-Osilyl species and binds to TiCl₄ to generate **Int26**, as a precursor for the next step. Cleavage of a silyl and chloride from **Int26** generates an intermediate **Int27** ready for cyclization. Cyclization in **Int27** is a kinetically and thermodynamically favorable process (Figure 17). The titanium in **TS16** has a trigonal bipyramidal geometry where two chlorides and an Oxo ligand lie in the plane of the

trigonal; however, the CH and chloride ligands are in the vertical axis. The CH-metal bond distance increases to 3.02 Å in the transition state from 2.22 Å in **Int27**. Moreover, the CH and keto carbon bond distance is 2.87 Å which indicates a very early transition state. The calculated activation barrier for the cyclization is 19.54 kcal mol⁻¹. Dehydration and tautomerization in **Int28** may deliver the final aromatic product.

1,4 addition

Int23 generated by the loss of a silyl chloride molecule can also undergo a 1,4 addition on the α, β unsaturated ketone to deliver intermediate **Int29** which is thermodynamically more stable than the intermediate **Int23** by 3.03 kcal mol⁻¹. The reaction has kinetic demand of 19.57 kcal mol⁻¹ which is higher than the kinetic demand for the 1,2 addition in **Int23'** (11.23 kcal mol⁻¹). These observations are also consistent with the theoretical calculations for the trifluoromethyl system (vide supra) where direct attack is more favourable than the 1,4 addition. From these calculations, one can infer that 1,2-addition is a more feasible pathway compared to 1,4-addition for these formal [3+3] addition reactions (1,4 addition). The difference in activation barrier for 1,2 and 1,4 attack is 8.34 kcal mol⁻¹ for the methyl system whereas this difference is about 7.9 kcal mol⁻¹ for the trifluoromethyl analogue.

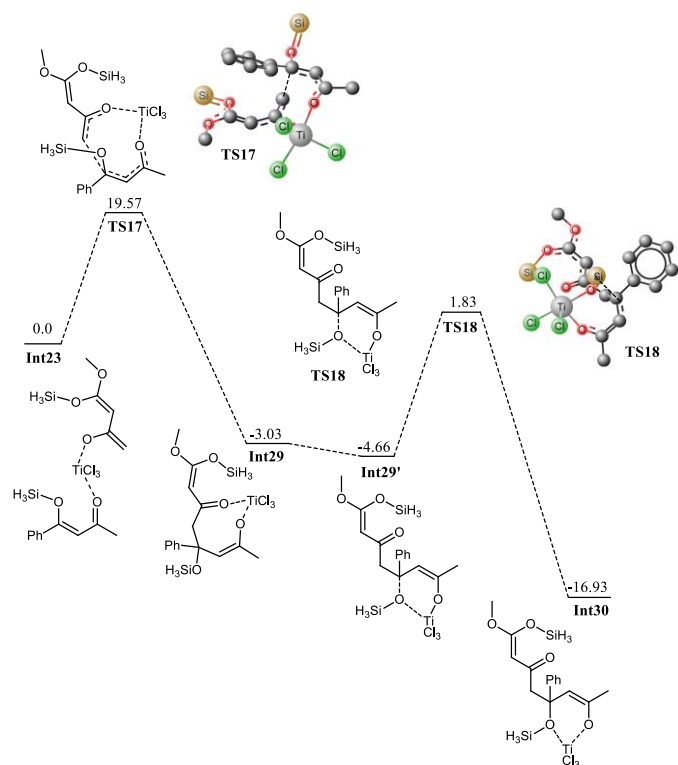


Figure 18. Potential energy diagram for Ti catalyzed 1,4 addition of enol to enone in **Int23**. All values in kcal mol⁻¹ with respect to **Int23** at 0.0 kcal mol⁻¹.

The subsequent cyclization has a calculated activation barrier of 19.72 kcal mol⁻¹ which is not significantly different than the one calculated for the cyclization in **Int27** which clearly illustrates that the selectivity is governed at the first addition step of the formal [3+3] addition reaction. The 1,2 addition (1,2 addition), shown in Figures 16 and 17, delivers the product with the experimentally observed regioselectivity. The 1,4 addition (shown in Figure 18) does not deliver the product with the correct regioselectivity. These findings are consistent with our the calculations that 1,2 addition is a favourable process with lower activation barriers compared to the 1,4 addition.

In summary, we have shown that the experimentally observed different regioselectivities for CH₃ and CF₃ enones can be explained by a common mechanism where 1,2 addition of 1,3-bis(silyl enol ethers) on 1,3-dielectrophiles is a more favorable pathway than the competing 1,4 addition. The differences in regioselectivities originate from different isomeric structures of enones entering in the catalytic cycle.

Conclusions

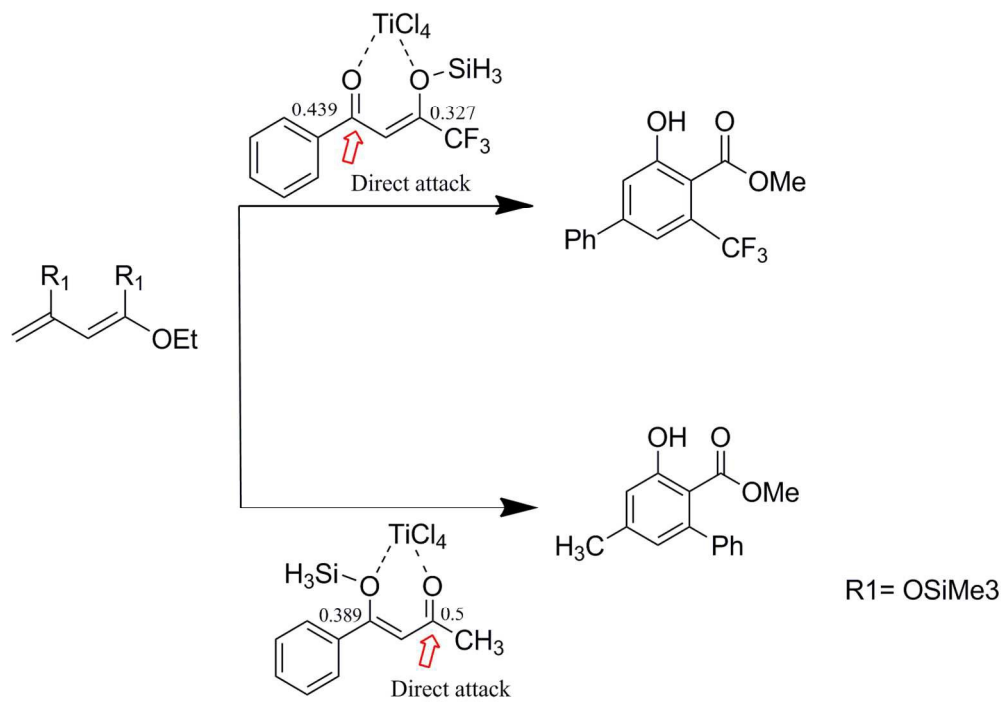
Density functional theory calculations have been performed to gain mechanistic insight of the formal [3+3] addition of 1,3-bis(silyl enol ethers) and 1,3-dielectrophiles to explain the experimentally observed regioselectivities. For this purpose, reaction of 1,3-bis(silyl enol ethers) with two different 1,3-dielectrophiles (**5** and **9**) is studied. The silyl moieties in 1,3-dielectrophiles are dynamic even in the absence of a metal catalyst ($E_{\text{act}} < 5$ kcal mol⁻¹). The isomeric dielectrophiles (for example **5** and **5'**) differ in their reactivity in formal [3+3] addition, and it depends on the strength of the positive charge (Mulliken charges) on the electrophilic carbon atom. Calculations reveal that a single mechanism can justify the experimentally observed different regioselectivities for **5** and **5'** depending on the isomeric species entering in the catalytic cycle (**11** and **12'**). 1,2 and 1,4 addition mechanisms have been studied for both isomeric forms of each dielectrophile. The calculations reveal that 1,2 addition of 1,3-bis(silyl enol ethers) on 1,3-dielectrophile is a favorable process over the conjugate (1,4) addition. A typical mechanism involves coordination of 1,3-bis(silyl enol ethers) and 1,3-dielectrophiles with TiCl₄ followed by elimination of Silyl chloride. The elimination of silyl chlorides has an activation barrier of about 19-20 kcal mol⁻¹. The elimination of the silyl chloride is followed by a nucleophilic attack on the dielectrophile. This nucleophilic addition governs the selectivity of the reaction. For trifluoromethyl, 1,2 addition (1,2 addition) is kinetically much favorable ($E_{\text{act}} = 5.2$ kcal mol⁻¹) than the 1,4 addition ($E_{\text{act}} = 13.1$ kcal mol⁻¹, Figure 18). For the methyl analogue, the difference in the activation barriers for the 1,2 and 1,4 addition is even more pronounced in the favor of 1,2 addition (about 8.34 kcal mol⁻¹). The trends in the activation barrier for 1,2 and 1,4 addition for both dielectrophiles can be correlated to Mulliken charges at the electrophilic centers.

Acknowledgements

The authors acknowledge the financial support from Higher Education Commission of Pakistan (Grant No. 1899), COMSATS Institute of Information Technology, and University of Rostock. This work has also been supported by the project "Light2Hydrogen" of the BMBF and the project "Nano4Hydrogen" of the ESF and the state of Mecklenburg-Vorpommern.

Notes and references

1. Nijveldt, R.J., et al., *The American journal of clinical nutrition*, 2001, **74**, 418-425.
2. Brunsveld, L., et al., *Chemical reviews*, 2001, **101**, 4071-4098.
3. Rappoport, Z., *The Chemistry of Phenols* 2004: John Wiley & Sons.
4. Langenaeker, W., K. Demel, and P. Geerlings, *Journal of Molecular Structure: THEOCHEM*, 1991, **234**, 329-342. (and reference herein)
5. Chupakhin, O.N., V.N. Charushin, and H.C. Van der Plas, *Nucleophilic aromatic substitution of hydrogen* 2012: Academic Press.
6. Miyaoura, N. and A. Suzuki, *Chemical reviews*, 1995, **95**, 2457-2483.
7. Karapetyan, G., et al., *Current Organic Chemistry*, 2012, **16**, 557-565.
8. Shkooor, G., 2010, M.Sc. Thesis.
9. Dötz, K. and P. Tomuschat, *Chemical Society Reviews*, 1999, **28**, 187-198.
10. Bonaga, L.V., et al., *Journal of the American Chemical Society*, 2005, **127**, 3473-3485.
11. Danheiser, R.L., et al., *Journal of the American Chemical Society*, 1990, **112**, 3093-3100.
12. Serra, S., C. Fuganti, and A. Moro, *The Journal of Organic Chemistry*, 2001, **66**, 7883-7888.
13. Bi, X., et al., *Journal of the American Chemical Society*, 2005, **127**, 4578-4579.
14. Feist, H. and P. Langer, *Synthesis*, 2007, **3**, 327-347.
15. Mukaiyama, T., *Angewandte Chemie International Edition in English*, 1977, **16**, 817-826.
16. Zhang, H.-H., et al., *Organic Letters*, 2014, **16**, 4896-4899.
17. Choudhary, P., et al., *Journal of Modern Chemistry and Applications*, 2012, **2013**, Article ID 1.
18. Bandini, M., et al., *Tetrahedron Letters*, 1999, **40**, 1997-2000.
19. Ramesha, S., H. Bhojya Naik, and H. Harish Kumar, *Journal of Sulfur Chemistry*, 2007, **28**, 573-579.
20. Narasaka, K., E. Bald, and T. Mukaiyama, *Chemistry Letters*, 1975, 1041-1044.
21. Gennari, C., et al., *Journal of the American Chemical Society*, 1985, **107**, 5812-5813.
22. Chan, T.-H. and P. Brownbridge, *Journal of the Chemical Society, Chemical Communications*, 1979, 578-579.
23. Specowius, V., et al., *Advanced Synthesis & Catalysis*, 2012, **354**, 1163-1169.
24. De Bruin, T.J., et al., *Organometallics*, 2003, **22**, 3404-3413.
25. Clark, R., *J. Chem. Soc.*, 1963, 1377-1384.
26. Clark, R., et al., *J. Chem. Soc.*, 1963, 379-387.



133x93mm (300 x 300 DPI)